Check for updates

Received: 24 January 2024 | Revised: 13 April 2024 | Accepted: 29 April 2024

DOI: 10.1002/ajpa.24952

TECHNICAL NOTE

AMERICAN JOURNAL OF BIOLOGICAL ANTHROPOLOGY
The Official Journal of the American Association of Biological Anthropologists

WILEY

# Technical note: Micro-computed tomography calibration using dental tissue for bone mineral research

Ian Towle[1,2] | Carolina Loch[2] | Marc Oxenham[3,4] | Kristin L. Krueger[5] | Amira Samir Salem[2] | Marina Martínez de Pinillos[1,6] | Mario Modesto-Mata[1,7] | Leslea J. Hlusko[1]

[1]Centro Nacional de Investigación sobre la Evolución Humana (CENIEH), Burgos, Spain

[2]Sir John Walsh Research Institute, Faculty of Dentistry, University of Otago, Dunedin, New Zealand

[3]School of Archaeology and Anthropology, Australian National University, Canberra, Australia

[4]Department of Archaeology, School of Geosciences, University of Aberdeen, Aberdeen, UK

[5]Department of Anthropology, Loyola University Chicago, Chicago, IL, USA

[6]Laboratorio de Evolución Humana (LEH), Universidad de Burgos, Burgos, Spain

[7]Universidad Internacional de La Rioja (UNIR), Logroño La Rioja, Spain

**Correspondence**
Ian Towle, Centro Nacional de Investigación sobre la Evolución Humana (CENIEH), Paseo Sierra de Atapuerca 3, 09002 Burgos, Spain.
Email: ianetowle@gmail.com

**Funding information**
Sir John Walsh Research Institute, University of Otago, Grant/Award Number: Sir Thomas Kay Sidey Postdoctoral fellowship; HORIZON EUROPE European Innovation Ecosystems, Grant/Award Numbers: ERC-2021-ADG, Tied2Teeth, 101054659

## Abstract

Computed tomography (CT) and microcomputed tomography (μCT) require calibration against density phantoms scanned with specimens or during routine internal calibration for assessment of mineral concentration (MC) and density. In clinical studies involving bone, alternative calibration methods using bodily tissues and fluids ("phantomless" calibration) have been suggested. However, such tissues are seldom available in archeological and osteological research. This study investigates the potential of dental tissue as internal reference for calibration of μCT scans, facilitating the analysis of bone MC. We analyzed 70 molars from 24 extant primate species, including eight human teeth, each scanned with density phantoms for calibration. Our findings indicate that sampling specific regions of molars (lateral aspects of the mesial cusps) yields low variation in enamel and dentine MC values, averaging 1.27 g/cm$^3$ (±0.03) for dentine and 2.25 g/cm$^3$ (±0.03) for enamel. No significant differences were observed across molar types or among scanning procedures, including scanner model, resolution, and filters. An ad hoc test on 12 mandibles revealed low variance in MC between the conventional phantom and dental tissue calibration methods; all 36 measurements (low, medium, and high MC for each mandible) were within 0.05 g/cm$^3$ of each other —81% were within 0.03 g/cm$^3$ and 94% within 0.04 g/cm$^3$. Based on these results, we propose a new "phantomless" calibration technique using these mean enamel and dentine MC values. The presented phantomless calibration method could aid in the assessment of bone pathology and enhance the scope of studies investigating bone structure and physical property variations in archeological, osteological, and laboratory-based research.

**KEYWORDS**
bone mineral concentration, micro-CT calibration, phantomless calibration, μCT

This is an open access article under the terms of the Creative Commons Attribution-NonCommercial-NoDerivs License, which permits use and distribution in any medium, provided the original work is properly cited, the use is non-commercial and no modifications or adaptations are made.
© 2024 The Authors. *American Journal of Biological Anthropology* published by Wiley Periodicals LLC.

## 1 | INTRODUCTION

Computed tomography (CT) scanning, a medical imaging technique that employs x-rays, is a versatile tool with numerous practical medical applications. While the diagnosis of conditions often relies on clinical expertise, in some instances the precise quantification of bone density values is needed. In particular, scan calibration plays a crucial role in evaluating bone pathologies causing changes in density and mineral content through time (Jaramillo et al., 2015; Nazarian et al., 2008; Richards et al., 2010; Telfer et al., 2021). The need for calibration extends to research involving in vivo imaging of model mammals and ex vivo scanning of tissues, where the accurate assessment of density and mineral content variations may be essential (Bart & Wallace, 2013; Beaucage et al., 2016; Bouxsein et al., 2010; Sevilla et al., 2015). The calibration process involves scanning materials of known-density and mineral content, called density phantoms or standards, alongside the sample, or alternatively, phantoms are scanned separately either as an initial calibration procedure or at regular time intervals (e.g., Loch et al., 2018; Schwass et al., 2009; Sevilla et al., 2015; Srirangapatanam et al., 2022).

Phantomless calibration techniques have emerged as viable alternatives in clinical settings. These innovative approaches enable the calibration of CT/microcomputed tomography (μCT) scans for the assessment of bone mineral content and density by using bodily fluids and/or soft tissues as a calibration reference, including blood, fat, and muscle (e.g., Bartenschlager et al., 2022; Bartenschlager et al., 2023; Gudmundsdottir et al., 1993; Lee et al., 2017; Pickhardt et al., 2011; Prado et al., 2021; Weaver et al., 2015). Bone mineral density refers to measurements taken concerning the adjacent soft tissue, such as the quantity of bone within a mixed region of bone and soft tissue. Consequently, it does not provide insights into the mineral content of bone in distinct areas. To address this terms such as "tissue mineral density" (TMD; Bouxsein et al., 2010; Kazakia et al., 2008), and "mineral concentration" (MC; Towle, Salem et al., 2023) are used when investigating a particular tissue type.

In nonmedical research, such as μCT and CT studies in osteology, archaeology, and paleontology, the assessment of bone MC is often not required. For instance, when examining tissue volume, size variation, or employing geometric morphometric techniques, calibration of scans is typically unnecessary (e.g., Lei et al., 2020; Pan et al., 2021; Skinner et al., 2010; Smith et al., 2012; Zhang et al., 2021). In these studies, the evaluation of tissue density is only needed during the initial tissue segmentation, where calibration methods are seldom required. Certain samples, particularly fossil and archeological in specific environmental contexts, have inherent challenges in MC estimation of bone or teeth due to taphonomic alterations (Towle et al., 2021; Wu & Schepartz, 2009). Nevertheless, there is potential for enhancing archeological and osteological studies with valuable MC data if a reliable and user-friendly calibration method can be established.

A promising solution to facilitate "phantomless" calibration of bone MC, applicable to both archeological and modern scenarios, entails using dental tissue as a reference material for calibration. Dental enamel, and to a lesser extent, dentine, are known for their consistently high mineral content and associated mechanical properties (Cuy et al., 2002; Loch et al., 2022; Park et al., 2008; Srirangapatanam et al., 2022). Nonetheless, several critical considerations need to be addressed before dental tissue can be used for phantomless μCT calibration of bone MC. A crucial factor is the variability observed in enamel and dentine, as even minor variations could introduce biases. However, recent research has highlighted the potential for consistency in MC values within specific enamel and dentine locations, provided that standardized data collection criteria are adhered to (Towle, Salem et al., 2023). This finding served as the impetus for the current study, which seeks to examine the feasibility and efficacy of a dental phantomless calibration method for bone MC research.

In this study, we use a streamlined recording scheme to minimize variability within tooth crown regions. Specifically, tooth regions with high variability in mineral content, such as outer and inner enamel/dentine locations and cusp tips, have been intentionally excluded from consideration. Subsequently, we evaluated this modified approach across molars sourced from various primate taxa, and different scanning protocols, in order to assess variability across samples. The overarching objective was to ascertain the feasibility of using teeth as a proxy for traditional density standards/phantoms when calibrating μCT scans for bone MC research. Our hypothesis posits that variations in MC will be low in these specific tooth locations, with no significant differences among species, commonly used scanning techniques, and/or molar tooth types, rendering this method practical for μCT calibration. However, should our hypothesis be refuted—confirming variability in MC values within specific enamel and dentin locations across various species, scanning techniques, and tooth types—it would suggest teeth may not be suitable for calibration of μCT scans.

## 2 | MATERIALS AND METHODS

### 2.1 | Samples

We examined a total of 70 molars, encompassing specimens from 21 Catarrhini and three Platyrrhini species. Only teeth that were free of macroscopic pathology and excessive tooth wear were selected. Here, excessive tooth wear is defined as the convergence of two or more dentine islands associated with each cusp on the occlusal surface. All specimens were scanned "dry" (i.e., osteological/museum specimens). Of the eight human teeth examined, two were obtained as extractions part of routine dental treatment with patient consent and had previously been stored at the University of Otago University Faculty of Dentistry teaching collection in 10% formalin solution. Both specimens were left to air dry for several days before scanning. The remaining human samples were archeological in nature, originating from sites in present day Philippines (site: Basco) and Northern Vietnam (site: Con co Co Nngua), and are curated at the Australian National University. One of the archeological samples, Con Cco

26927691, 0, Downloaded from https://onlinelibrary.wiley.com/doi/10.1002/ajpa.24952 by Universidad De Burgos, Wiley Online Library on [23/05/2024]. See the Terms and Conditions (https://onlinelibrary.wiley.com/terms-and-conditions) on Wiley Online Library for rules of use; OA articles are governed by the applicable Creative Commons License

Nngua, was associated with a hunter-gatherer population that lived around 6800–6200 years ago in what is now Northern Vietnam. This site, placed within a broader regional and temporal framework, has been extensively examined in the literature (e.g., Jones et al., 2019; Oxenham, 2006; Oxenham et al., 2018; Scott et al., 2019; Vlok et al., 2022). The other site, Basco, located on Batan island, Northern Philippines, is not dated. However, teeth were recovered from a jar burial and are believed to predate European contact (see Bellwood & Dizon, 2013). Both clinical extracted and archeological human teeth were µCT scanned at the Otago Micro and Nanoscale Imaging facility before being returned to the original collections.

The non-human primate samples are curated at the Primate Research Institute (PRI) (now the Center for the Evolutionary Origins of Human Behavior), Kyoto University, Japan, and from several museum collections within New Zealand: Auckland Museum (Auckland), University of Otago (Faculty of Dentistry, Dunedin), Otago Museum (Dunedin), and the Dunedin Museum of Natural Mystery (Dunedin). Considering all samples, most are from Cercopithecidae (species: 15; samples: 46), followed by Hominoidea (species: 6; samples: 18, including 8 human molars), and a smaller sample of Platyrrhini (species: 3; samples: 6). The SOM details each sample, including species, tooth type, sex (if known), place of curation, and the settings used for scanning (summarized below). The data that supports the findings of this study are also available in the Supplementary material.

## 2.2 | Data collection

Two different µCT scanners were used in this study, one at the PRI (SkyScan1275) and one at the University of Otago (Skyscan1172). Different filters and resolutions were used for these two machines. Whole jaws (maxilla/whole skull and mandibles) scanned at PRI were scanned at lower resolution, and the individual teeth scanned at the University of Otago were scanned at higher resolution. The main differences in settings/filters are summarized in Table 1. For individual tooth samples, specimens were positioned with all cusps facing upward, ensuring approximate horizontal evenness. The teeth were inserted into a thin plastic tube positioned directly above the density phantoms before being placed in the scanning chamber. When teeth were scanned within jaws, molars were oriented with cusps facing approximately vertical, and the phantoms were positioned directly above or below the teeth.

Resin-hydroxyapatite phantoms were used to calibrate grayscales and MC in each specimen, following Schwass et al. (2009). Calibration and data collection were undertaken in ImageJ (Schneider et al., 2012). Hounsfield unit (HU) is proportional to the degree of x-ray attenuation by the tissue, which is displayed as greyscale values. Grayscale values were recorded on each of the three phantoms using 3 mm diameter circular regions of interest (ROI's), with three positions recorded every 10 slices (total of 10 slices; ROI $n = 30$). Scans were then calibrated using the "calibrate" function in ImageJ, in which the mean grayscale reflects the known MC values for each disk (i.e., creating a linear regression used to calibrate scans). After calibration with the phantoms, buccal and lingual MC ROI locations within the mesial cusps of molars were studied in each specimen.

These locations were chosen because they showed relatively consistent values across a small sample of Catarrhini lower molars in a recent study (Towle, Salem et al., 2023). Data were collected on five slices of the lateral enamel (Figure 1). The five slices were spaced approximately evenly from the top of the lateral enamel down to where the enamel tapers to the cementum enamel junction (Figure 1). Dentine readings were recorded on the same five slices. Each of the five slices therefore had four ROI readings, two buccal and two lingual locations (enamel and dentine). A circular ROI of varying diameter was placed in the middle of the enamel area (halfway between the enamel–dentine junction [EDJ] and the outer enamel surface). The

**TABLE 1** A comparison of scanners, filters, and reconstruction settings used in this study.

| Scanning location | Skyscan1172 | SkyScan1275 |
|---|---|---|
| Resolution | Higher resolution | Lower resolution |
| µCT scanner model | University of Otago | PRI, Japan |
| Isotropic voxel size (µm) | 15 | 44 |
| Filter | Al + Cu | Cu 1 mm |
| Beam hardening correction (%) | 80 | 30 |
| Ring artifact correction | 15 | 10 |
| Smoothing | 5 | 3 |
| Source voltage (kV) | 100 | 100 |
| Source current (uA) | 100 | 100 |
| Rotation step (deg) | 0.2 | 0.2 |
| Reconstruction angular range (deg) | 360 | 360 |

Abbreviations: PRI, Primate Research Institute; µCT, microcomputed tomography.

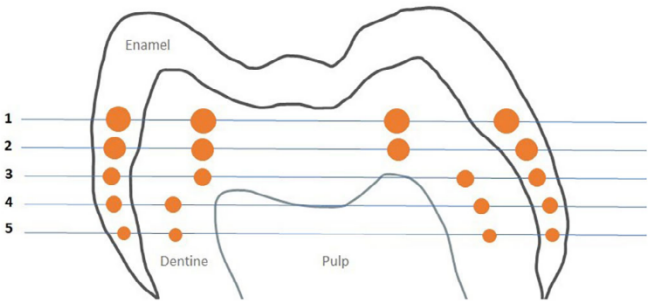


**FIGURE 1** Schematic representation of slice positions for collecting 20 region of interest (ROI) values per specimen. The shown slice is through the mesial cusps (lingual to buccal), with ROI diameter size approximately half the enamel thickness, using an average between buccal and lingual locations for each slice. Note that the ROI size was consistent within each slice but varied among the five slices and across specimens.

26927691, 0, Downloaded from https://onlinelibrary.wiley.com/doi/10.1002/ajpa.24952 by Universidad De Burgos, Wiley Online Library on [23/05/2024]. See the Terms and Conditions (https://onlinelibrary.wiley.com/terms-and-conditions) on Wiley Online Library for rules of use; OA articles are governed by the applicable Creative Commons License

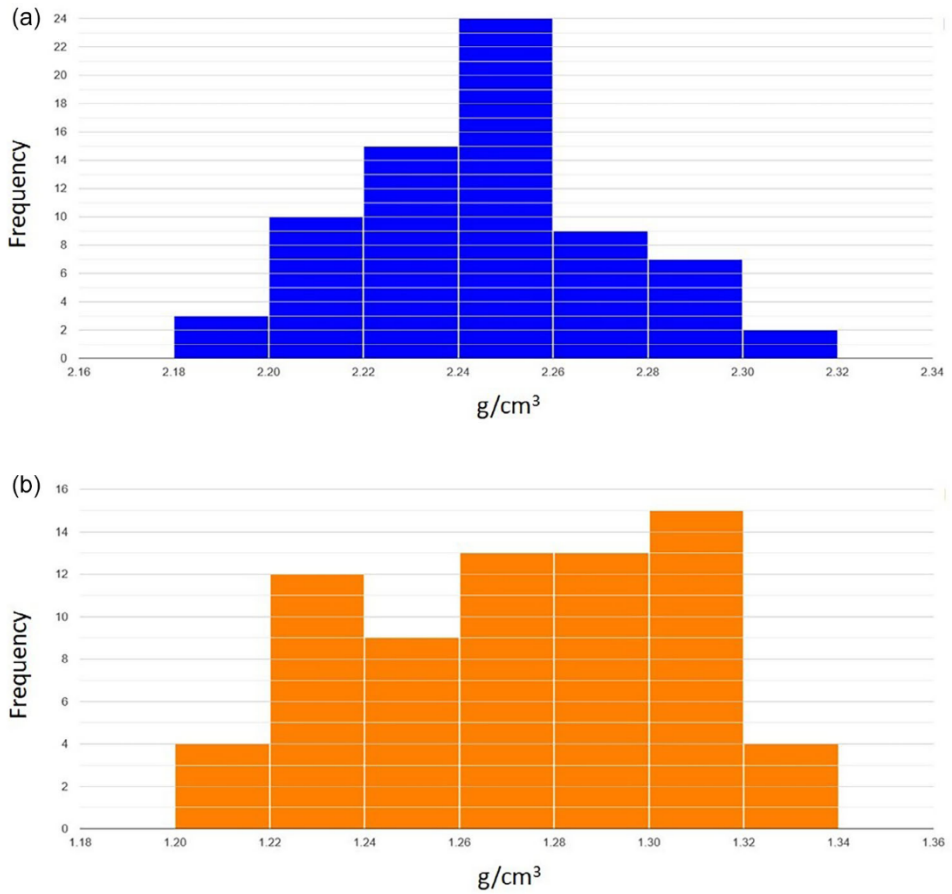


**FIGURE 2** Histograms showing the distribution of molar mineral concentration average values for each sample for enamel (a) and dentine (b).

size of the ROI varied across the five slices so it filled approximately half the width of the enamel (Figure 1). This same ROI size was used for dentine. The ROI was placed in the 'middle' of the dentine in each slice, which means halfway between the EDJ and the pulp chamber when present, and halfway to the middle of the tooth when not present (Figure 1). This generates 10 enamel and 10 dentine ROI values for each tooth, from which, an overall average for both dental tissues were calculated. Areas close to the mesial/distal midpoint of the cusps were selected, but locations mesial or distal to this were used if there were obvious scanning artifacts in these regions.

**TABLE 2** A Levene's test was performed to calculate the homogeneity of variances assumption for different subsamples. Bold indicates significant variance.

| Groups | Enamel | Dentine |
|---|---|---|
| Higher resolution and lower resolution | $F(1,68) = 1.34$, $p = 0.251$ | $F(1,68) = 0.06$, $p = 0.805$ |
| Maxilla and mandible | **$F(1,68) = 9.07$, $p = 0.004$** | $F(1,68) = 0.019$, $p = 0.892$ |
| M1, M2, and M3 | $F(2,67) = 0.39$, $p = 0.677$ | $F(2,67) = 0.79$, $p = 0.458$ |

## 2.3 | Statistical analysis

Statistical analysis was performed to evaluate variations among tooth types and scanning settings. In all analyses, mean enamel and dentine values for each specimen were used. To assess the distribution of the samples, a Kolmogorov–Smirnov test of normality was employed. When assessing variance using the average values for enamel and dentine in each sample ($n = 70$ in each case), no significant deviations from a normal distribution were observed (Enamel: $D(70) = 0.06$, $p = 0.923$; Dentine: $D(70) = 0.10$, $p = 0.402$; Figure 2).

To test for differences between scanning methods and tooth types, a Welch's *t*-test and independent-samples *t*-test were performed. The comparisons involved unequal sample sizes and the potential for unequal variances between the groups, and in some cases, relatively small sample sizes. Given these considerations, Welch's *t*-test was considered the most suitable choice. However, in all but one of the comparisons (as determined by Levene's test; see Table 2), the variances were reasonably equal. Therefore, we present both the results of the independent-samples *t*-test (assuming equal variances) and Welch's *t*-test (considering unequal variances) to provide a comprehensive analysis. There were no differences in results between these two statistical approaches. A Pearson correlation coefficient was employed to determine whether there was a statistically significant correlation between enamel and dentine values across all samples.

26927691, 0, Downloaded from https://onlinelibrary.wiley.com/doi/10.1002/ajpa.24952 by Universidad De Burgos, Wiley Online Library on [23/05/2024]. See the Terms and Conditions (https://onlinelibrary.wiley.com/terms-and-conditions) on Wiley Online Library for rules of use; OA articles are governed by the applicable Creative Commons License

## 2.4 | Phantomless calibration technique

To assess the practicality of the phantomless calibration method employing dental tissues, an ad hoc analysis was conducted utilizing the average enamel and dentine values obtained in this study. Bone MC was measured in the 12 µCT scans that included entire mandibles. In each scan, three discrete MC values were extracted, representing the low, medium, and high MC ranges, for both the traditional phantom and the new phantomless calibration methods. These three values were established by identifying the approximate range of cortical bone MC within two slices from two benchmark mandibles (see Figure 6), defined as follows: low MC at 0.6 g/cm$^3$, medium MC at 1.0 g/cm$^3$, and high MC at 1.4 g/cm$^3$. Grayscale values correlating to these MC standards were first obtained using the established phantom-based calibration approach. Subsequent recalibration was performed using the phantomless technique to derive MC values for the identical grayscale indices. A mean value for all studied teeth within each mandible was used to generate the mean dentine and enamel values. The deviation between the two calibration techniques was quantified for each MC category across the 12 mandibles.

## 3 | RESULTS

There was little variation in enamel or dentine MC across the 70 teeth studied (dentine average value: 1.27 g/cm$^3$ ± 0.03; enamel average value 2.25 g/cm$^3$ ± 0.03; Figure 3). The average dentine and enamel values were also similar among maxillary and mandibular molars (maxillary teeth, dentine: 1.27 g/cm$^3$ ± 0.04, enamel: 2.25 g/cm$^3$ ± 0.02; mandibular teeth, dentine: 1.27 g/cm$^3$ ± 0.03, enamel: 2.25 g/cm$^3$ ± 0.03); among first, second, and third molars (first molars, dentine: 1.27 g/cm$^3$ ± 0.03, enamel: 2.24 g/cm$^3$ ± 0.02; second

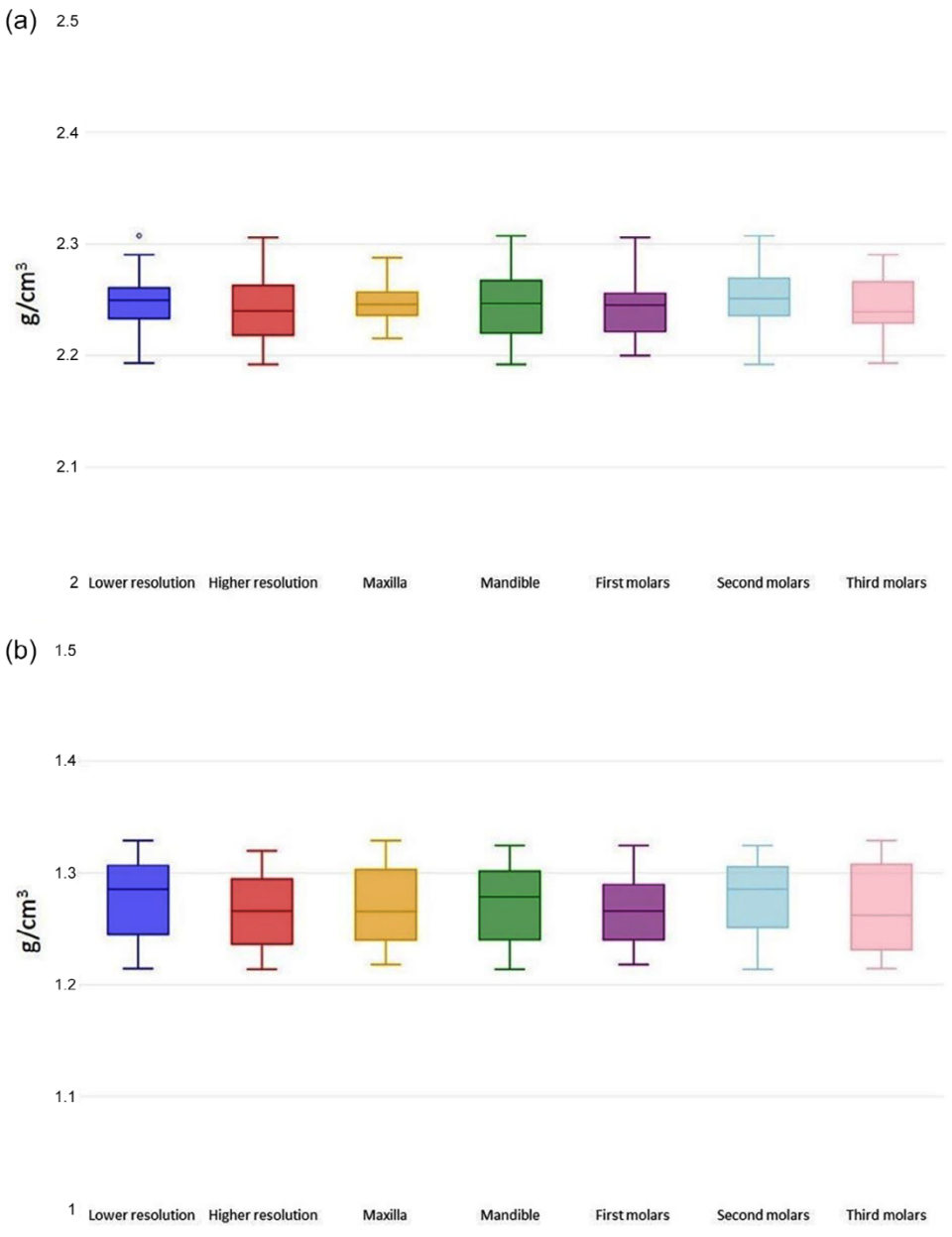


**FIGURE 3** Box and whisker plots showing the variance in mineral concentration (g/cm$^3$), split into different subsamples for enamel (a) and dentine (b). Lower resolution refers to all Primate Research Institute (PRI) scanned samples, and higher resolution the University of Otago samples (see text for further details). Sample sizes: lower resolution ($N = 45$), higher resolution ($N = 25$), maxilla ($N = 21$), mandible ($N = 49$), first molars ($N = 25$), second molars ($N = 33$), third molars ($N = 12$).

26927691, 0, Downloaded from https://onlinelibrary.wiley.com/doi/10.1002/ajpa.24952 by Universidad De Burgos, Wiley Online Library on [23/05/2024]. See the Terms and Conditions (https://onlinelibrary.wiley.com/terms-and-conditions) on Wiley Online Library for rules of use; OA articles are governed by the applicable Creative Commons License

**TABLE 3** Statistical comparisons utilizing independent-samples *t*-test and Welch's *t*-test to evaluate differences among tooth types and scanning methodologies.

| Comparison | Enamel | Dentine |
|---|---|---|
| Independent-samples *t*-test | | |
| Higher resolution Vs. lower resolution | $t(44,24) = 0.77$, $p = 0.442$ | $t(44,24) = 1.39$, $p = 0.170$ |
| Maxilla Vs. mandible | $t(20,48) = 0.26$, $p = 0.796$ | $t(20,48) = -0.11$, $p = 0.912$ |
| M1 Vs. M2 | $t(24,32) = -1.05$, $p = 0.300$ | $t(24,32) = -1.52$, $p = 0.135$ |
| M1 Vs. M3 | $t(24,11) = -0.18$, $p = 0.855$ | $t(24,11) = -0.14$, $p = 0.887$ |
| M2 Vs. M3 | $t(32,11) = 0.59$, $p = 0.560$ | $t(32,11) = 0.94$, $p = 0.351$ |
| Welch's *t*-test | | |
| Higher resolution Vs. lower resolution | $t(42.4013) = 0.73$, $p = 0.468$ | $t(51.4283) = 1.40$, $p = 0.166$ |
| Maxilla versus mandible | $t(63.1558) = 0.32$, $p = 0.749$ | $t(35.9648) = -0.11$, $p = 0.915$ |
| M1 versus M2 | $t(55.2451) = -1.07$, $p = 0.289$ | $t(53.9917) = -1.54$, $p = 0.130$ |
| M1 versus M3 | $t(18.1053) = -0.17$, $p = 0.866$ | $t(17.2095) = -0.13$, $p = 0.899$ |
| M2 versus M3 | $t(18.7185) = 0.57$, $p = 0.573$ | $t(16.751) = 0.86$, $p = 0.402$ |

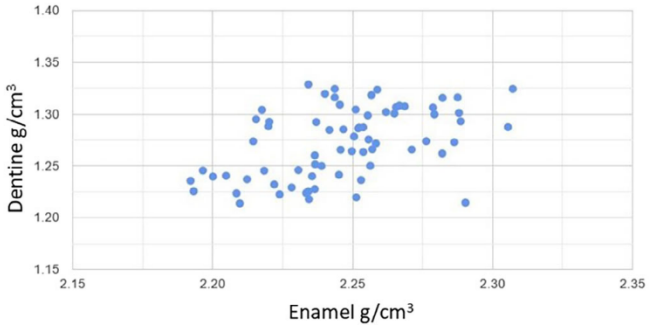


**FIGURE 4** Scatter plot of 70 mineral concentration (MC) values (average for whole tooth) for enamel and dentine. A significant relationship between enamel and dentine MC was found ($r(68) = 0.476$, $p < 0.001$).

molars, dentine: 1.28 g/cm$^3$ ± 0.03, enamel: 2.25 g/cm$^3$ ± 0.03; third molars, dentine: 1.27 g/cm$^3$ ± 0.04, enamel: 2.24 g/cm$^3$ ± 0.03), and between the different scanning methodologies (PRI scanner/settings: dentine: 1.28 g/cm$^3$ ± 0.03, enamel: 2.25 g/cm$^3$ ± 0.02; University of Otago: dentine: 1.26 g/cm$^3$ ± 0.03, enamel: 2.24 g/cm$^3$ ± 0.03). There were no clear differences between males and females or between taxonomic groups, but due to uncertainty of the sex of many of the specimens (see SOM), and limited sample sizes for some taxa, further comparisons were not possible.

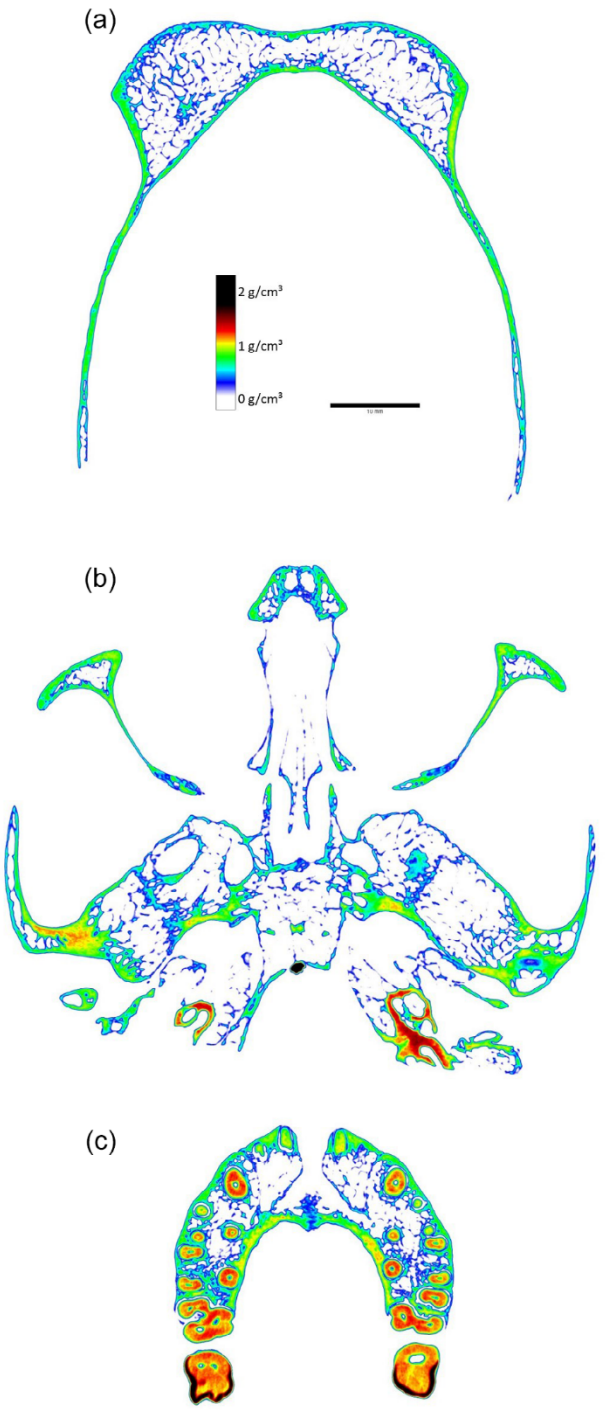


**FIGURE 5** Microcomputed tomography (μCT) scan calibrated (in ImageJ) using the enamel and dentine average values (enamel: 2.25 g/cm$^3$; dentine: 1.27 g/cm$^3$). Species: *Simias concolor* (PRI 1248). Three slices of the same skull, approximate horizontal slices considering the skull in upright vertical position, with anterior facing upward in all cases. (a) Near the top of the skull, with the top of the supraorbital torus visible; (b) approximately halfway through the scan, with various skull bones visible; (c) maxilla, with bone, dentine and enamel visible.

The statistical analysis results show no significant differences based on tooth type (first to third molars, maxilla/mandible) and between scanning methodology (Table 3). Results of the Pearson correlation coefficient indicated that there is a significant medium

26927691, 0, Downloaded from https://onlinelibrary.wiley.com/doi/10.1002/ajpa.24952 by Universidad De Burgos, Wiley Online Library on [23/05/2024]. See the Terms and Conditions (https://onlinelibrary.wiley.com/terms-and-conditions) on Wiley Online Library for rules of use; OA articles are governed by the applicable Creative Commons License

positive relationship between enamel and dentine readings ($r(68) = 0.476$, $p < 0.001$; Figure 4). Figure 5 illustrates an example (specimen: *Simias concolor*: PRI 1248) to visualize a calibrated scan using the average enamel and dentine values for all specimens combined for calibration, showing bone MC within the expected ranges (i.e., <0.5 to ~1.5 g/cm$^3$; Figure 5).

The ad hoc analysis conducted in this study used mean values of enamel and dentine to assess the variation between the newly developed phantomless calibration technique and the conventional phantom-based method. Our examination of 12 mandibles indicated that MC values derived using the phantomless technique align closely with those obtained from the traditional method, as evidenced in Figures 6–8. Notably, variations in MC across low, medium, and high categories remained under the 0.05 g/cm$^3$ threshold when compared with phantom-based values, achieving 81% and 94% accuracy within the more stringent limits of 0.03 and 0.04 g/cm$^3$, respectively. We observed an increased disparity in regions with lower bone MC (Figure 8), consistent with their greater

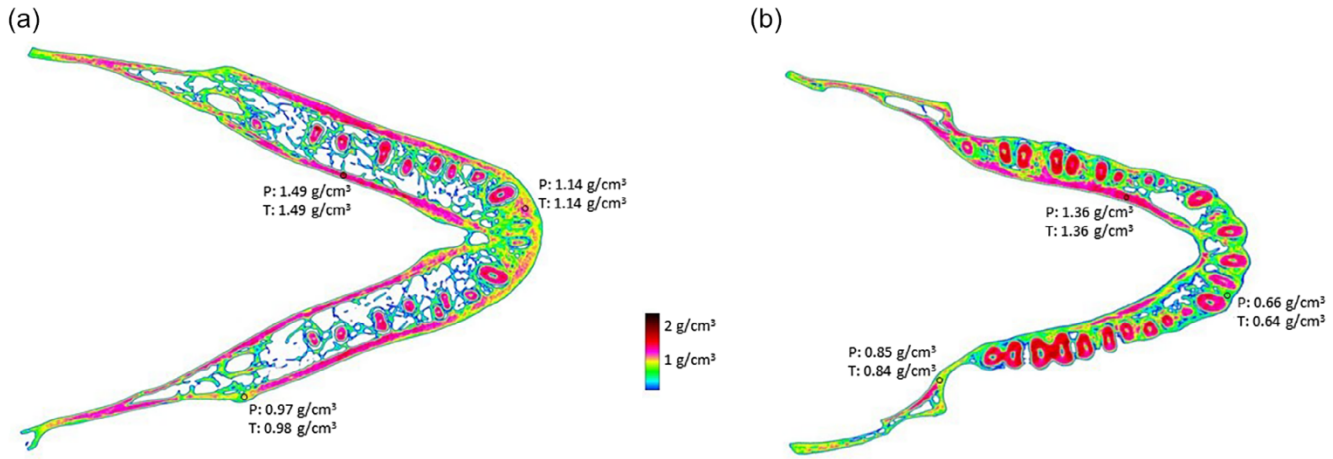


**FIGURE 6** Microcomputed tomography slice of two baboon mandibles, showing the difference in mineral concentration values for the same locations using two different calibration methods, P: conventional phantom calibration; T: dental tissue calibration. (a) PRI 1217; (b) PRI 11588.

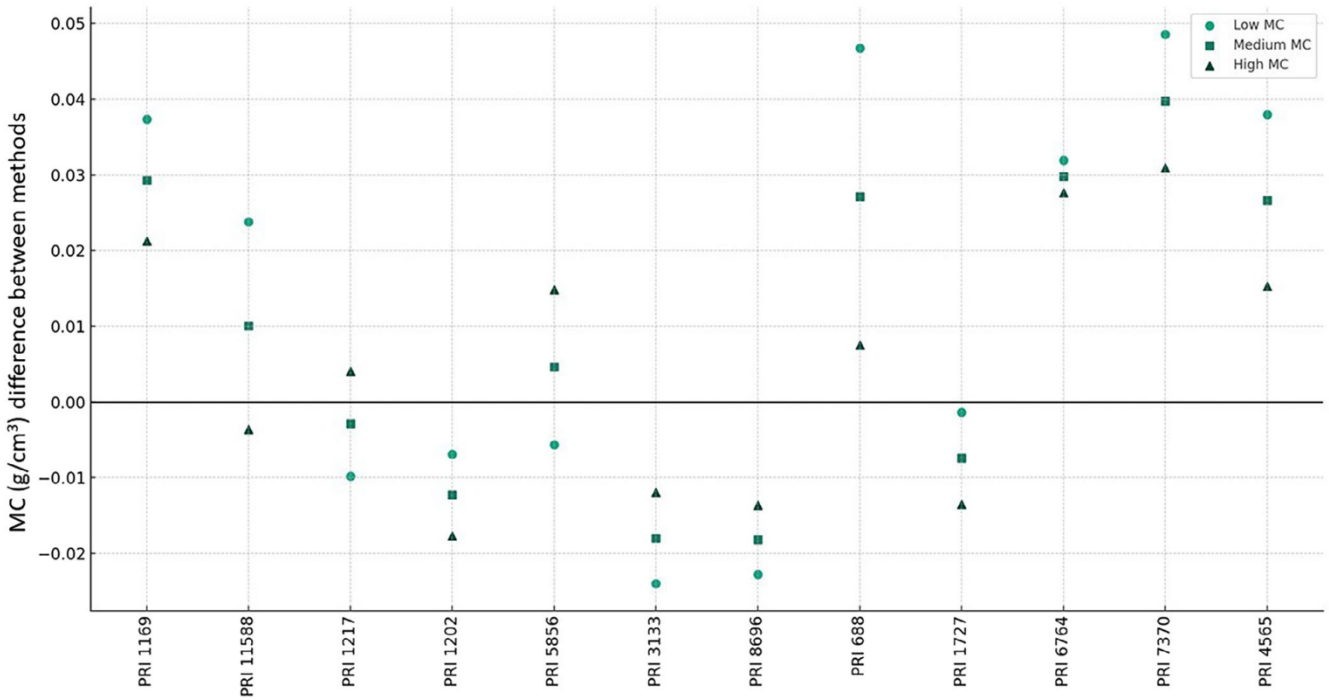


**FIGURE 7** Scatter plot highlighting the comparison of mineral concentration (MC) values across the 12 mandibles studied. Each point represents an individual MC estimate, with separate markers indicating low (circles), medium (squares), and high (triangles) MC categories (see text for details). The plot illustrates the distribution of MC values derived from the new "phantomless" calibration technique in relation to the values obtained from conventional phantom-based calibration.

26927691, 0, Downloaded from https://onlinelibrary.wiley.com/doi/10.1002/ajpa.24952 by Universidad De Burgos, Wiley Online Library on [23/05/2024]. See the Terms and Conditions (https://onlinelibrary.wiley.com/terms-and-conditions) on Wiley Online Library for rules of use; OA articles are governed by the applicable Creative Commons License

distance from the MC of the calibration materials adopted here (enamel and dentine).

## 4 | DISCUSSION

The results of this study support the view that enamel and dentine have uniform MC values across molar types and primate species when specific ROI locations on the lateral positions of the mesial cusps are recorded. No significant differences were observed between scanner types, resolution, and filter settings. Furthermore, there were no discernible differences among tooth types sampled (including upper and lower first to third molars), taxonomic groups, or sample preservation (modern and archeological), indicating the reliability and robustness of these values. Therefore, by following strict data collection methodology, dental tissues from molars yield MC values within a narrow range, with a standard deviation of 0.03 g/cm$^3$ for both enamel and dentine. An analysis of MC in the 12 mandibles in the present study found consistency between values obtained from conventional phantom methods and the new "phantomless" calibration technique. Differences across a range of MC values remained under 0.05 g/cm$^3$, with 81% of readings showing less than 0.03 g/cm$^3$ difference between the two techniques. Therefore, an enamel value of 2.25 g/cm$^3$ and a dentine value of 1.27 g/cm$^3$ can serve as reliable data points for calibrating µCT scans for bone research (i.e., phantom-equivalent measurements of MC).

The variation in MC in the phantoms used here may be even less than found in the tooth positions in the present study (i.e., standard deviation of 0.01 g/cm$^3$ for phantoms vs. 0.03 g/cm$^3$ for dental tissue; this study; Schwass et al., 2009). However, both methods show low variation, including compared with other tooth crown locations (e.g., when all locations are combined in (Towle, Salem et al., 2023) the standard deviation was 0.08 g/cm$^3$ for dentine and 0.11 g/cm$^3$ for enamel), and even more so compared to bone (i.e., ranging from under 0.5 g/cm$^3$ to over 1.5 g/cm$^3$ even within individual bone elements; Figures 5, 6, 9). Moreover, the standard deviation of 0.03 g/cm$^3$ in this study incorporates the phantoms' variance, since they were used for the initial calibration. This suggests that the actual variance in the proposed phantomless calibration method is likely lower than the reported value of 0.03 g/cm$^3$, and perhaps closer to the variance observed in the phantoms.

Multiple types of software and methodologies can effectively implement this calibration approach. In this section, we illustrate the method using ImageJ (Schneider et al., 2012), but other software can be equally applicable. To calibrate µCT scans using this phantomless calibration method, the same procedural steps as outlined in the Materials and Methods section were followed, however, instead of recording 20 ROI MC values from calibrated scans, grayscale values are recorded (as depicted in Figure 9a). It is critical to adhere to the specified ROI locations detailed above, in the lateral buccal and lingual areas within the mesial cusps, as MC values may fluctuate significantly in other crown regions (Towle, Salem et al., 2023). From the 20 ROI values, an average grayscale value for both dentine and enamel is then calculated. Subsequently, scans can be calibrated using the "calibrate" function within ImageJ. In this process, the mean grayscale values of enamel and dentine are placed in the left-hand column, and 2.25 and 1.27 placed in the right-hand column (Figure 9b). Once this calibration step is completed, the scan will be prepared for the collection of MC data of bone (ROI examples provided in Figure 9c).

Creating reliable phantoms for CT analysis of osteological and archeological skeletal material is a complex task. It involves developing materials with density and MC similar to bone and dental tissue, graded from low to high (Loch et al., 2018; Schwass et al., 2009; Srirangapatanam et al., 2022). Typically, this requires the creation of two to five density standards to scan alongside samples. The choice of methodologies and materials used can influence results. The primary parameter examined is x-ray absorption, quantified as the attenuation coefficient in units of 1/distance (mm$^{-1}$). This coefficient is influenced by both mass density and elemental composition. Ideally, these standards should match the MC range of the material under study and have a similar composition. In the context of bone, dentine, and enamel, it is assumed that x-ray attenuation is determined by

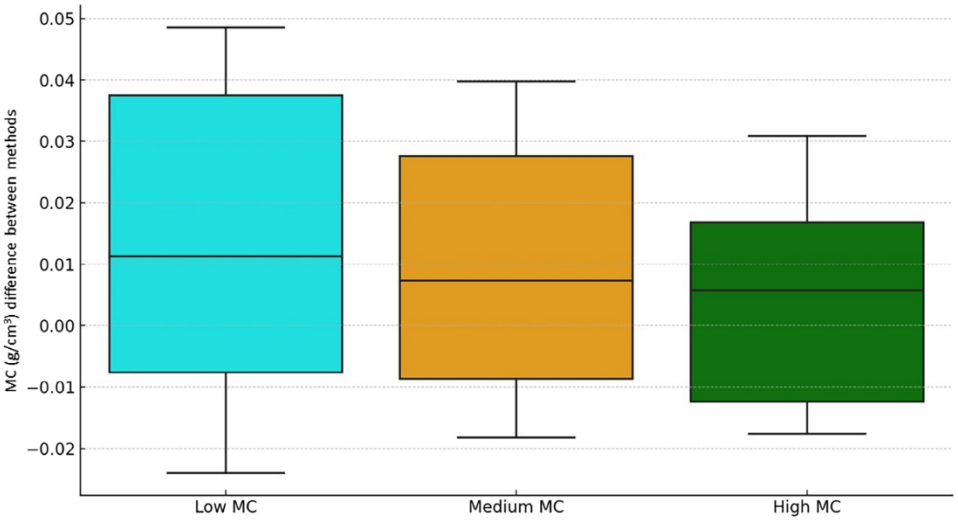


**FIGURE 8** Box plot outlining the deviations in mineral concentration (MC) values between the phantom-based and "phantomless" calibration methods for the same set of 12 mandibles. The boxes represent the interquartile ranges (IQR) for low (cyan), medium (orange), and high (green) MC categories, with the central line marking the median deviation. Whiskers extend to the furthest data points within 1.5 times the IQR from the box. No outliers were identified.

26927691, 0, Downloaded from https://onlinelibrary.wiley.com/doi/10.1002/ajpa.24952 by Universidad De Burgos, Wiley Online Library on [23/05/2024]. See the Terms and Conditions (https://onlinelibrary.wiley.com/terms-and-conditions) on Wiley Online Library for rules of use; OA articles are governed by the applicable Creative Commons License

calcium hydroxyapatite ($Ca_5(PO_4)_3(OH)$). Therefore, our methodologies are only suitable for materials composed of calcium hydroxyapatite. Furthermore, although enamel tends to have higher MC values than bone, dentine falls within the range of bone values (e.g., see Figures 5 and 6). Dental tissue therefore serves as ideal "natural" calibration materials for studying bone.

The results of our study closely mirror those of comparable investigations, especially in terms of dentine and enamel measurements (He et al., 2010; He et al., 2011; Song et al., 2017; Srirangapatanam et al., 2022; Towle, Salem et al., 2023). Nevertheless, direct comparisons are constrained due to variations in data collection locations and protocols. In a broader context, mineralization values for non-pathological dental tissues exhibit variability across diverse techniques, emphasizing the need for caution when comparing findings from different methodologies (Clementino-Luedemann & Kunzelmann, 2006; Davis & Wong, 1996; Djomehri et al., 2015; Srirangapatanam et al., 2022). Tooth preservation is critical, particularly when teeth are scanned "wet" (e.g., immediately after extraction or stored in liquid). While the minimal non-mineral content of dental tissue should not greatly affect MC values, variations in tissue surroundings can influence results (e.g., the scanning medium, such as water, saline, ethanol, or air (Bouxsein et al., 2010)). This was corroborated by a study on rats (Akbulut et al., 2020), where MC decreased slightly over time. Kazakia et al. (2008) found that mineralization measures obtained from μCT scans, while slightly underestimated, strongly correlate with other techniques such as synchrotron radiation μCT and gravimetric methods. Therefore, although the values generated from our calibration technique (and other studies using phantoms) may be slightly lower than values obtained from other, non-CT techniques, the results are reliable for studying natural and pathological variations in MC.

A major limitation of this calibration method is that the bone specimen being scanned will typically need to include the dentition. As a result, this method may mainly be applicable to craniofacial research. However, in some cases, an associated extracted or loose molar could be used alongside bone samples, or for batch calibration, making this method potentially more broadly applicable in specific circumstances. Additionally, this technique could also be used to calibrate scans lacking dental tissue by utilizing comparable scans that do include teeth, assuming both were performed under consistent conditions. These conditions include using the same scanner and scanning settings, and that the scans have been performed within a similar timeframe. This approach mirrors routine internal calibration practices seen in clinical CT settings, in which grayscale values produced across scans are comparable if the above criterion is followed. Therefore, if a scan containing teeth is calibrated, other similar "toothless" scans can potentially utilize the same calibration values. This new method could enable historical μCT data to be reevaluated, enhancing the scope and applicability of existing μCT datasets for exploring bone pathologies, conducting structural analyses, and studying physical properties in osteological collections.

In this study, we observed minimal variation in MC values among samples and tooth types; however, a significant relationship was found between enamel and dentine across the samples. This suggests

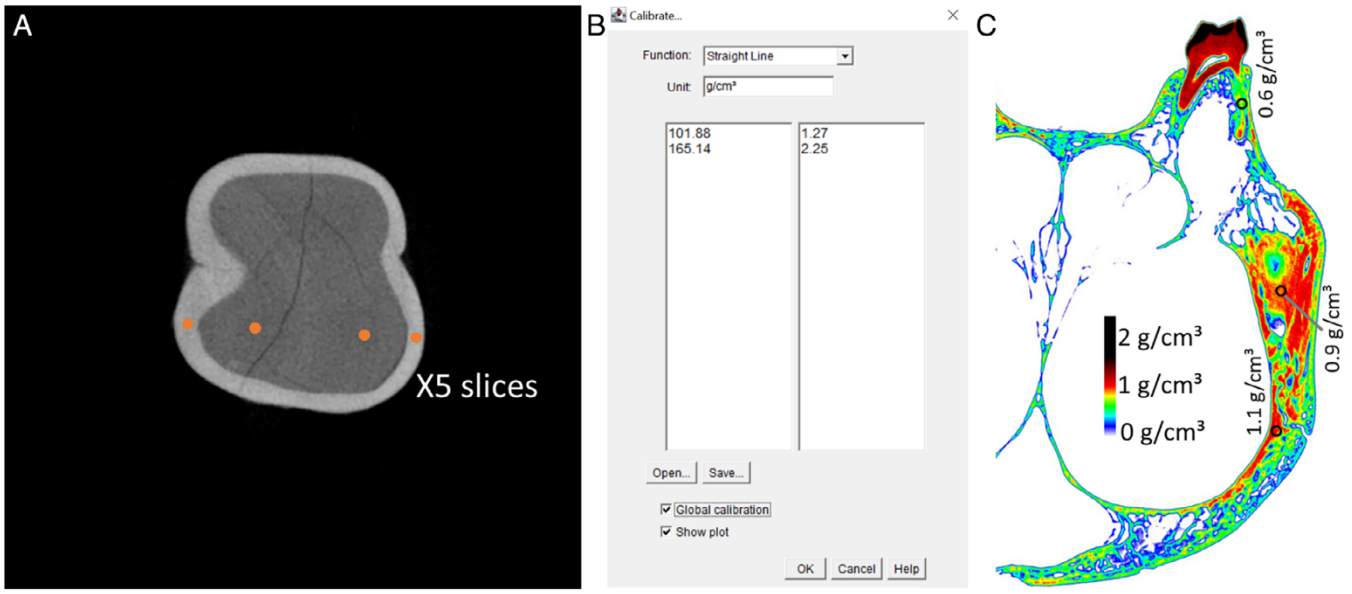


**FIGURE 9** A simplified representation of how bone mineral concentration (MC) values can be collected using the calibration method outlined in this study: (a) collect two enamel and dentine region of interest (ROI) grayscale values, one on the buccal side of the lateral mesial cusps and the other on the lingual side (then repeat for an additional four slices). (b) From these 10 enamel and 10 dentine values, calculate the mean grayscale value for each. Then click Analyze/Calibrate in ImageJ, and put the average mean grayscale value for enamel and dentine in the left column (generated by the average ROI values), and the known MC values from the present study (enamel value: 2.25 g/cm$^3$; dentine value: 1.27 g/cm$^3$) in the right column. Select straight line "Function" and select "Global calibration." Click OK and the scan is now calibrated for g/cm$^3$. (c) a ROI can now be selected in bone to give an average MC for that area (three examples shown). Specimen: *Macaca fascicularis* (PRI 280).

26927691, 0, Downloaded from https://onlinelibrary.wiley.com/doi/10.1002/ajpa.24952 by Universidad De Burgos, Wiley Online Library on [23/05/2024]. See the Terms and Conditions (https://onlinelibrary.wiley.com/terms-and-conditions) on Wiley Online Library for rules of use; OA articles are governed by the applicable Creative Commons License

that specimens with higher enamel values have higher dentine readings. While this might imply small genuine differences in MC across samples, this seems improbable given the absence of significant distinctions among tooth types or specimens. Instead, this relationship is more likely attributed to minor scanning effects. Considering the narrow range of MC values across the samples, even minor scanning artifacts could result in slight increases or decreases in the recorded MC values, affecting both enamel and dentine similarly (e.g., due to ring artifacts and beam hardening). This reinforces the notion that MC variation in these tooth positions, spanning various tooth types, wear stages, and species, is generally low to the extent that very minor scanning effects (e.g., changes <0.05 $mm^3$) are discernible in the data. Nonetheless, it underscores the importance of monitoring such factors, particularly when scans indicate severe scanning artifacts.

The calibration method proposed here relies solely on two data points—one from enamel and one from dentine. Consequently, even minor deviations can exert a more pronounced influence on the calibration. In addition to excluding teeth that exhibit extensive scanning effects (such as ring artifacts or inadequately corrected beam hardening), it is vital to refrain from selecting teeth with pathologies, hypo or hyper mineralization, and to adhere to the specific positions outlined here. It is also advisable to avoid teeth displaying enamel defects or significant discoloration, as these may be linked to hypomineralization (Davis & Wong, 1996; Hattab et al., 1999; Kammoun et al., 2019). Towle, Salem et al., (2023) highlighted subtle yet meaningful distinctions among specific crown positions, including cusps having higher values than lateral positions. Similar investigations have unveiled variations in MC, structure, and mechanical properties across tooth crowns, encompassing small-scale variations within enamel and more extensive differences between crown locations (e.g., Angker et al., 2004; Campbell et al., 2012; Cuy et al., 2002; Darnell et al., 2010; Huang et al., 2010; Mahoney et al., 2004; Towle, Loho et al., 2023). Hence, adopting a random approach when selecting ROIs from various crown locations for calibration may increase the risk of errors being introduced.

Different scanning settings and protocols can significantly impact density results, and the elimination of disparities between scanners remains challenging (Bart & Wallace, 2013). While our study did not uncover significant differences between scanner types, filters, resolution, and sample size, it is apparent that such disparities could be observed under different conditions. In this study, the use of commonly employed filters and scanning settings was slightly modified for the two scanners to enhance scan quality (e.g., to minimize scanning artifacts). Although different filters were used between scanners, they likely served similar purpose. In the absence of filters or without appropriate beam-hardening/ring artifact correction, significant differences among samples would likely emerge. Hence, it is imperative to implement appropriate scanning and reconstruction settings based on individual scanners and specimens when using the phantomless calibration technique.

Maintaining consistency in methods, such as the standardization of settings and filters (e.g., Free et al., 2018), is also essential to limit biases in results. Scan quality can vary widely in µCT scans, especially in relation to "noise" produced. This can be linked to the age of the scanner and artifacts such as debris in the chamber, or in association with different filters and settings used. When scans are affected by artifacts and noise, the methods outlined here may not be suitable. This is particularly pertinent in paleopathology studies, where the focus is often on the MC variation within a particular ROI in the same individual. Researchers should exercise caution when comparing µCT scans from different machines, with different settings, and varying noise levels. In particular, small differences in MC between individuals or populations may not reflect genuine variation in the samples, but rather differences in scanners, scan settings and artifact levels.

It is also important to record multiple ROI per tooth, as was done here (10 enamel and 10 dentine readings). Although the mean MC value for each tooth studied was similar, individual ROI can vary within a single tooth. For examle, the highest and lowest enamel ROI readings for individual teeth typically varied by 0.1–0.2 $mm^3$, and in some cases by a greater difference. This variation is related to genuine differences in MC (e.g., differences among buccal and lingual locations), but also to small variations in noise and artifacts produced among scans. Recording multiple ROI is therefore crucial and can minimize these effects.

On a larger scale, MC values obtained can be influenced not only by the reconstruction settings adopted but also by the specimen's placement within the chamber and its orientation (Entezari et al., 2012). In our current study, all specimens were positioned in the center of the chamber and with the same vertical orientation. It is crucial to keep this positioning in mind when applying the calibration techniques proposed here. As with other studies employing phantomless calibration, it is also essential to account for changes in the tissues over time. For example, skeletal muscle, as suggested by Bartenschlager et al. (2022), may not be the ideal choice for phantomless calibration due to age-related variations such as fatty infiltration in older individuals. This concern can extend to teeth, where both enamel and dentine can undergo MC changes during an individual's lifetime. Dentine has greater variability in MC and mechanical properties over time. New dentine formation gradually occurs throughout an individual's life (as secondary dentine) or in response to factors such as caries or extensive tooth wear (as tertiary dentine (Dean, 2017; Ricucci et al., 2014; Rutherford et al., 1995; Towle, 2019)). Enamel properties also vary during an individual's lifetime (e.g., Park et al., 2008). To address these variations, our methodology draws insights from existing literature. This involves excluding inner and outer locations in enamel, and dentine near the pulp chamber and EDJ. Additionally, excluding substantially worn teeth minimizes age-related changes.

The suitability of MC recording in different bone types depends on the scan resolution. For instance, a voxel size of approximately 10 µm is advisable for examining diaphyseal cortical bone in mice, but falls short for scrutinizing individual trabeculae or the thin cortex in metaphyseal regions (Bouxsein et al., 2010). However, in larger animals, Bouxsein et al. (2010) suggest that MC (referred to as TMD in their study) measurements within trabecular bone might be achievable, provided there are at least three voxels within the trabeculae. This approach is applicable to many skeletal locations in primates, but

26927691, 0, Downloaded from https://onlinelibrary.wiley.com/doi/10.1002/ajpa.24952 by Universidad De Burgos, Wiley Online Library on [23/05/2024]. See the Terms and Conditions (https://onlinelibrary.wiley.com/terms-and-conditions) on Wiley Online Library for rules of use; OA articles are governed by the applicable Creative Commons License

often requires higher resolution (isotropic voxel size) scans. Nevertheless, MC measurements of cortical bone in primates tend to be straightforward for most individuals and species, even with lower µCT voxel sizes. Achieving a balance between scanning resolution and scan time is a consideration dependent on the objectives of the study in question.

It is also worth noting that this technique can be used in samples from a range of time periods, from modern materials, through recent archeological collections (last few hundred years; e.g., Basco), to much older samples (thousands of years old; e.g., Con co Co Nngua). This calibration method could also prove useful in clinical and laboratory research, although further research is required to understand MC variability in enamel and dentine in posterior teeth of other mammals, and in a larger sample of extracted human teeth (Akbulut et al., 2020; Chugh et al., 2013). Common applications encompass both in vivo imaging of small animals and ex vivo scanning of tissues, with diverse uses including the study of disease, organ structure, and drug treatments (Bart & Wallace, 2013; Guldberg et al., 2003; Pasetto et al., 2018; Ritman, 2004). Further research is required to assess the suitability of using similar dental calibration methods in other taxonomic groups.

## 5 | CONCLUSION

This study demonstrates the feasibility of using dental tissue, specifically enamel and dentine, as an internal calibration reference material for µCT scans, enabling the assessment of bone MC without the need for conventional density phantoms. Enamel and dentine MC values have minimal variation across primate species, scanner types, resolution, and filters used in lateral positions of mesial molar cusps. This phantomless calibration technique offers a valuable tool for the investigation of bone pathology and the analysis of density variations in osteological, archeological, and potentially veterinary/laboratory research contexts. The ease of implementation of this method and consistency across samples makes it a practical alternative to conventional phantom-based calibration, with potential applications to other research fields. However, data collection criteria need to be consistent and consider factors such as tooth wear and changes in dental tissue composition over time. Additionally, the suitability of MC recording in different bone types and specific regions depends on scan resolution, and careful consideration of scanning settings is necessary for each study. Despite these limitations, this study offers a valuable new approach for enhancing bone data that can be collected from µCT scans.

## AUTHOR CONTRIBUTIONS

**Ian Towle:** Conceptualization (lead); data curation (lead); formal analysis (lead); funding acquisition (equal); investigation (lead); methodology (lead); project administration (equal); visualization (lead); writing – original draft (lead); writing – review and editing (lead). **Carolina Loch:** Formal analysis (supporting); funding acquisition (equal); investigation (supporting); methodology (supporting); project administration (supporting); writing – original draft (supporting); writing – review and editing (equal). **Marc Oxenham:** Formal analysis (supporting); investigation (supporting); methodology (supporting); project administration (supporting); resources (supporting); writing – original draft (supporting); writing – review and editing (equal). **Kristin L. Krueger:** Formal analysis (supporting); investigation (supporting); methodology (supporting); visualization (supporting); writing – original draft (supporting); writing – review and editing (equal). **Amira Samir Salem:** Formal analysis (supporting); investigation (supporting); methodology (supporting); writing – original draft (supporting); writing – review and editing (equal). **Marina Martínez de Pinillos:** Formal analysis (supporting); investigation (supporting); methodology (supporting); writing – original draft (supporting); writing – review and editing (equal). **Mario Modesto-Mata:** Formal analysis (supporting); investigation (supporting); methodology (supporting); writing – original draft (supporting); writing – review and editing (equal). **Leslea J. Hlusko:** Formal analysis (supporting); funding acquisition (equal); investigation (supporting); methodology (supporting); project administration (supporting); writing – original draft (supporting); writing – review and editing (equal).

## ACKNOWLEDGMENTS

Collection of the µCT scans was supported by a Sir Thomas Kay Sidey Postdoctoral fellowship from the Faculty of Dentistry, University of Otago, to Ian Towle. We thank staff and facilities of the Otago Micro and Nanoscale Imaging for assistance with Micro-CT scanning. This research was additionally facilitated by the European Research Council within the European Union's Horizon Europe (ERC-2021-ADG, Tied2-Teeth, project number 101054659). The authors thank the Study Material Committee from the Primate Research Institute (PRI), Kyoto University, for access to their collections, and T. Ito for assistance during data collection. The research was performed under the Cooperative Research Program of the PRI (2019-C-20). We also thank the museums in New Zealand that provided samples for this study and the curators for their assistance and support, including Otago Museum (E. Burns), Dunedin Museum of Natural Mystery (B. Mahalski), and Auckland Museum (M. Rayner and R. Moore). Last, we thank A. Hara for helpful discussions during the inception of this study. The authors have no conflict of interests to declare. Open access publishing facilitated by University of Otago, as part of the Wiley - University of Otago agreement via the Council of Australian University Librarians.

## DATA AVAILABILITY STATEMENT

The data that supports the findings of this study are available in the supplementary material.

## ORCID

*Ian Towle* https://orcid.org/0000-0002-0939-7222
*Marc Oxenham* https://orcid.org/0000-0002-5804-2145
*Kristin L. Krueger* https://orcid.org/0000-0002-8132-7675

## REFERENCES

Akbulut, N., Çetin, S., Bilecenoğlu, B., Altan, A., Akbulut, S., Ocak, M., & Orhan, K. (2020). The micro-CT evaluation of enamel-cement thickness, abrasion, and mineral density in teeth in the postmortem interval

26927691, 0, Downloaded from https://onlinelibrary.wiley.com/doi/10.1002/ajpa.24952 by Universidad De Burgos, Wiley Online Library on [23/05/2024]. See the Terms and Conditions (https://onlinelibrary.wiley.com/terms-and-conditions) on Wiley Online Library for rules of use; OA articles are governed by the applicable Creative Commons License

(PMI): New parameters for the determination of PMI. *International Journal of Legal Medicine*, *134*, 645–653.

Angker, L., Nockolds, C., Swain, M. V., & Kilpatrick, N. (2004). Quantitative analysis of the mineral content of sound and carious primary dentine using BSE imaging. *Archives of Oral Biology*, *49*(2), 99–107.

Bart, Z. R., & Wallace, J. M. (2013). Microcomputed tomography applications in bone and mineral research. *Advances in Computed Tomography*, *02*, 121–127.

Bartenschlager, S., Cavallaro, A., Pogarell, T., Chaudry, O., Uder, M., Khosla, S., Schett, G., & Engelke, K. (2023). Opportunistic screening with CT: Comparison of phantomless BMD calibration methods. *Journal of Bone and Mineral Research*, *38*, 1689–1699.

Bartenschlager, S., Dankerl, P., Chaudry, O., Uder, M., & Engelke, K. (2022). BMD accuracy errors specific to phantomless calibration of CT scans of the lumbar spine. *Bone*, *157*, 116304.

Beaucage, K. L., Pollmann, S. I., Sims, S. M., Dixon, S. J., & Holdsworth, D. W. (2016). Quantitative in vivo micro-computed tomography for assessment of age-dependent changes in murine whole-body composition. *Bone Reports*, *5*, 70–80.

Bellwood, P., & Dizon, E. (2013). *4000 years of migration and cultural exchange: The archaeology of the Batanes Islands* (p. 254). ANU Press.

Bouxsein, M. L., Boyd, S. K., Christiansen, B. A., Guldberg, R. E., Jepsen, K. J., & Müller, R. (2010). Guidelines for assessment of bone microstructure in rodents using micro–computed tomography. *Journal of Bone and Mineral Research*, *25*(7), 1468–1486.

Campbell, S. E., Cuozzo, F. P., Sauther, M. L., Sponheimer, M., & Ferguson, V. L. (2012). Nanoindentation of lemur enamel: An ecological investigation of mechanical property variations within and between sympatric species. *American Journal of Physical Anthropology*, *148*(2), 178–190.

Chugh, T., Jain, A. K., Jaiswal, R. K., Mehrotra, P., & Mehrotra, R. (2013). Bone density and its importance in orthodontics. *Journal of Oral Biology and Craniofacial Research*, *3*(2), 92–97.

Clementino-Luedemann, T. N. R., & Kunzelmann, K. H. (2006). Mineral concentration of natural human teeth by a commercial micro-CT. *Dental Materials Journal*, *25*(1), 113–119.

Cuy, J. L., Mann, A. B., Livi, K. J., Teaford, M. F., & Weihs, T. P. (2002). Nanoindentation mapping of the mechanical properties of human molar tooth enamel. *Archives of Oral Biology*, *47*(4), 281–291.

Darnell, L. A., Teaford, M. F., Livi, K. J., & Weihs, T. P. (2010). Variations in the mechanical properties of Alouatta palliata molar enamel. *American Journal of Physical Anthropology*, *141*(1), 7–15.

Davis, G. R., & Wong, F. S. (1996). X-ray microtomography of bones and teeth. *Physiological Measurement*, *17*(3), 121–146.

Dean, C. (2017). How the microstructure of dentine can contribute to reconstructing developing dentitions and the lives of hominoids and hominins. *Comptes Rendus Palevol*, *16*(5–6), 557–571.

Djomehri, S. I., Candell, S., Case, T., Browning, A., Marshall, G. W., Yun, W., Lau, S. H., Webb, S., & Ho, S. P. (2015). Mineral density volume gradients in normal and diseased human tissues. *PLoS One*, *10*(4), e0121611.

Entezari, V., Vartanians, V., Zurakowski, D., Patel, N., Fajardo, R. J., Müller, R., Snyder, B. D., & Nazarian, A. (2012). Further improvements on the factors affecting bone mineral density measured by quantitative micro-computed tomography. *Bone*, *50*(3), 611–618.

Free, J., Eggermont, F., Derikx, L., van Leeuwen, R., van der Linden, Y., Jansen, W., Raaijmakers, E., Tanck, E., & Kaatee, R. (2018). The effect of different CT scanners, scan parameters and scanning setup on Hounsfield units and calibrated bone density: A phantom study. *Biomedical Physics & Engineering Express*, *4*(5), 055013.

Gudmundsdottir, H., Jonsdottir, B., Kristinsson, S., Johannesson, A., Goodenough, D., & Sigurdsson, G. J. O. I. (1993). Vertebral bone density in Icelandic women using quantitative computed tomography without an external reference phantom. *Osteoporosis International*, *3*, 84–89.

Guldberg, R. E., Ballock, R. T., Boyan, B. D., Duvall, C. L., Lin, A. S. P., Nagaraja, S., Oest, M., Phillips, J., Porter, B. D., Robertson, G., & Taylor, W. R. (2003). Analyzing bone, blood vessels, and biomaterials with microcomputed tomography. *IEEE Engineering in Medicine and Biology*, *22*(5), 77–83.

Hattab, F. N., Qudeimat, M. A., & AL-RIMAWI, H. S. (1999). Dental discoloration: An overview. *Journal of Esthetic and Restorative Dentistry*, *11*(6), 291–310.

He, B., Huang, S., Jing, J., & Hao, Y. (2010). Measurement of hydroxyapatite density and Knoop hardness in sound human enamel and a correlational analysis between them. *Archives of Oral Biology*, *55*(2), 134–141.

He, B., Huang, S., Zhang, C., Jing, J., Hao, Y., Xiao, L., & Zhou, X. (2011). Mineral densities and elemental content in different layers of healthy human enamel with varying teeth age. *Archives of Oral Biology*, *56*(10), 997–1004.

Huang, T. T., He, L. H., Darendeliler, M. A., & Swain, M. V. (2010). Correlation of mineral density and elastic modulus of natural enamel white spot lesions using X-ray microtomography and nanoindentation. *Acta Biomaterialia*, *6*(12), 4553–4559.

Jaramillo, J. D., Wilson, C., Stinson, D. J., Lynch, D. A., Bowler, R. P., Lutz, S., Bon, J. M., Arnold, B., McDonald, M.-L. N., Washko, G. R., Wan, E. S., DeMeo, D. L., Foreman, M. G., Soler, X., Lindsay, S. E., Lane, N. E., Genant, H. K., Silverman, E. K., Hokanson, J. E., … COPDGene Investigators. (2015). Reduced bone density and vertebral fractures in smokers. Men and COPD patients at increased risk. *Annals of the American Thoracic Society*, *12*(5), 648–656.

Jones, R. K., Piper, P. J., Groves, C. P., Anh, T. N., Thi, M. H. N., Thị, H. N., Hoang, T. H., & Oxenham, M. F. (2019). Shifting subsistence patterns from the terminal Pleistocene to late Holocene: A regional southeast Asian analysis. *Quaternary International*, *529*, 47–56.

Kammoun, R., Zmantar, T., Labidi, A., Abbes, I., Mansour, L., & Ghoul-Mazgar, S. (2019). Dental caries and hypoplastic amelogenesis imperfecta: Clinical, structural, biochemical and molecular approaches. *Microbial Pathogenesis*, *135*, 103615.

Kazakia, G. J., Burghardt, A. J., Cheung, S., & Majumdar, S. (2008). Assessment of bone tissue mineralization by conventional x-ray microcomputed tomography: Comparison with synchrotron radiation microcomputed tomography and ash measurements. *Medical Physics*, *35*(7Part1), 3170–3179.

Lee, D. C., Hoffmann, P. F., Kopperdahl, D. L., & Keaveny, T. M. (2017). Phantomless calibration of CT scans for measurement of BMD and bone strength—Inter-operator reanalysis precision. *Bone*, *103*, 325–333.

Lei, P. A. N., Wei, L. I. A. O., Wei, W. A. N. G., Jianhui, L. I. U., Xueping, J. I., Xiaomei, Y. A. N. G., & Yixin, H. A. O. (2020). Geometric morphometry of the enamel-dentine junction interface of Lufengpithecus hudienensis lower fourth premolars. *Acta Anthropologica Sinica*, *39*(4), 555.

Loch, C., Hemm, L., Taylor, B., Visser, I. N., & Wiig, Ø. (2022). Microstructure, elemental composition and mechanical properties of enamel and dentine in the polar bear Ursus maritimus. *Archives of Oral Biology*, *134*, 105318.

Loch, C., Schwass, D. R., Kieser, J. A., & Fordyce, R. E. (2018). *Use of micro-computed tomography for dental studies in modern and fossil odontocetes: Potential applications and limitations* (p. 10). NAMMCO Scientific Publications.

Mahoney, E. K., Rohanizadeh, R., Ismail, F. S. M., Kilpatrick, N. M., & Swain, M. V. (2004). Mechanical properties and microstructure of hypomineralised enamel of permanent teeth. *Biomaterials*, *25*(20), 5091–5100.

Nazarian, A., Snyder, B. D., Zurakowski, D., & Müller, R. (2008). Quantitative micro-computed tomography: A non-invasive method to assess equivalent bone mineral density. *Bone*, *43*(2), 302–311.

Oxenham, M. (2006). Biological responses to change in prehistoric Viet Nam. *Asian Perspectives*, *45*, 212–239.

26927691, 0, Downloaded from https://onlinelibrary.wiley.com/doi/10.1002/ajpa.24952 by Universidad De Burgos, Wiley Online Library on [23/05/2024]. See the Terms and Conditions (https://onlinelibrary.wiley.com/terms-and-conditions) on Wiley Online Library for rules of use; OA articles are governed by the applicable Creative Commons License

Oxenham, M. F., Trinh, H. H., Willis, A., Jones, R. K., Domett, K., Castillo, C., Wood, R., Bellwood, P., Tromp, M., Kells, A., Piper, P., Pham, S. T., Matsumura, H., & Buckley, H. (2018). Between foraging and farming: Strategic responses to the Holocene thermal maximum in Southeast Asia. *Antiquity*, *92*(364), 940–957.

Pan, L., Ji, X., Liao, W., Wang, W., Liu, J., & Xing, S. (2021). Premolar enamel thickness and distribution of a Miocene hominid *Lufengpithecus hudienensis* compared with Pleistocene and extant hominids. *Journal of Human Evolution*, *157*, 103030.

Park, S., Wang, D. H., Zhang, D., Romberg, E., & Arola, D. (2008). Mechanical properties of human enamel as a function of age and location in the tooth. *Journal of Materials Science: Materials in Medicine*, *19*, 2317–2324.

Pasetto, L., Olivari, D., Nardo, G., Trolese, M. C., Bendotti, C., Piccirillo, R., & Bonetto, V. (2018). Micro-computed tomography for non-invasive evaluation of muscle atrophy in mouse models of disease. *PLoS One*, *13*(5), e0198089.

Pickhardt, P. J., Lee, L. J., Muñoz del Rio, A., Lauder, T., Bruce, R. J., Summers, R. M., Pooler, B. D., & Binkley, N. (2011). Simultaneous screening for osteoporosis at CT colonography: Bone mineral density assessment using MDCT attenuation techniques compared with the DXA reference standard. *Journal of Bone and Mineral Research*, *26*(9), 2194–2203.

Prado, M., Khosla, S., Chaput, C., & Giambini, H. (2021). Opportunistic application of phantom-less calibration methods for fracture risk prediction using QCT/FEA. *European Radiology*, *31*(12), 9428–9435.

Richards, A. M., Coleman, N. W., Knight, T. A., Belkoff, S. M., & Mears, S. C. (2010). Bone density and cortical thickness in normal, osteopenic, and osteoporotic sacra. *Journal of Osteoporosis*, *2010*, 1–5.

Ricucci, D., Loghin, S., Lin, L. M., Spångberg, L. S., & Tay, F. R. (2014). Is hard tissue formation in the dental pulp after the death of the primary odontoblasts a regenerative or a reparative process? *Journal of Dentistry*, *42*(9), 1156–1170.

Ritman, E. L. (2004). Micro-computed tomography—current status and developments. *Annual Review of Biomedical Engineering*, *6*, 185–208.

Rutherford, B., Spångberg, L., Tucker, M., & Charette, M. (1995). Transdentinal stimulation of reparative dentine formation by osteogenic protein-1 in monkeys. *Archives of Oral Biology*, *40*(7), 681–683.

Schneider, C. A., Rasband, W. S., & Eliceiri, K. W. (2012). NIH image to ImageJ: 25 years of image analysis. *Nature Methods*, *9*(7), 671–675.

Schwass, D. R., Swain, M. V., Purton, D. G., & Leichter, J. W. (2009). A system of calibrating microtomography for use in caries research. *Caries Research*, *43*(4), 314–321.

Scott, R. M., Buckley, H. R., Domett, K., Tromp, M., Trinh, H. H., Willis, A., Matsumura, H., & Oxenham, M. F. (2019). Domestication and large animal interactions: Skeletal trauma in northern Vietnam during the hunter-gatherer Da but period. *PLoS One*, *14*(9), e0218777.

Sevilla, R. S., Cruz, F., Chiu, C. S., Xue, D., Bettano, K. A., Zhu, J., Chakravarthy, K., Faltus, R., Wang, S., Vanko, A., Robinson, G., Zielstorff, M., Miao, J., Leccese, E., Conway, D., Moy, L. Y., Dogdas, B., Cicmil, M., & Zhang, W. (2015). Development and optimization of a high-throughput micro-computed tomography imaging method incorporating a novel analysis technique to evaluate bone mineral density of arthritic joints in a rodent model of collagen induced arthritis. *Bone*, *73*, 32–41.

Skinner, M. M., Evans, A., Smith, T., Jernvall, J., Tafforeau, P., Kupczik, K., Olejniczak, A. J., Rosas, A., Radovcić, J., Thackeray, J. F., Toussaint, M., & Hublin, J. J. (2010). Brief communication: Contributions of enamel-dentine junction shape and enamel deposition to primate molar crown complexity. *American Journal of Physical Anthropology*, *142*(1), 157–163.

Smith, T. M., Olejniczak, A. J., Zermeno, J. P., Tafforeau, P., Skinner, M. M., Hoffmann, A., Radovčić, J., Toussaint, M., Kruszynski, R., Menter, C., Moggi-Cecchi, J., Glasmacher, U. A., Kullmer, O., Schrenk, F., Stringer, C., & Hublin, J. J. (2012). Variation in enamel thickness within the genus *Homo*. *Journal of Human Evolution*, *62*(3), 395–411.

Song, D. S., Kim, J. W., Hwang, H. S., Oh, S. H., Song, J. H., Kim, I. S., Hwang, Y.-C., & Koh, J. T. (2017). Quantitative analysis of tooth mineral content by high resolution micro-computed tomography. *International Journal of Oral Biology*, *42*(4), 155–161.

Srirangapatanam, S., Kang, M., Ellenikiotis, Y., Jheon, A., Kapila, S., Swana, H. S., Stoller, M. L., Seo, Y., & Ho, S. P. (2022). Standardization of mineral density maps of physiologic and pathologic biominerals in humans using cone-beam CT and micro-CT scanners. *Dental Materials*, *38*(6), 989–1003.

Telfer, S., Kleweno, C. P., Hughes, B., Mellor, S., Brunnquell, C. L., Linnau, K. F., & Hebert-Davies, J. (2021). Changes in scapular bone density vary by region and are associated with age and sex. *Journal of Shoulder and Elbow Surgery*, *30*(12), 2839–2844.

Towle, I. (2019). Tertiary dentine frequencies in extant great apes and fossil hominins. *Open Quaternary*, *5*(1), p. 2.

Towle, I., Irish, J. D., Groote, I. D., Fernée, C., & Loch, C. (2021). Dental caries in south African fossil hominins. *South African Journal of Science*, *117*(3–4), 1–8.

Towle, I., Loho, T., Salem, A. S., Berthaume, M. A., & Loch, C. (2023). Variation in enamel mechanical properties throughout the crown in catarrhine primates. *Journal of Human Evolution*, *182*, 103413.

Towle, I., Salem, A. S., Veneziano, A., & Loch, C. (2023). Variation in enamel and dentine mineral concentration and density in primate molars. *Archives of Oral Biology*, *153*, 105752.

Vlok, M., Buckley, H. R., Domett, K., Willis, A., Tromp, M., Trinh, H. H., Minh, T. T., Mai Huong, N. T., Nguyen, L. C., Matsumura, H., Huu, N. T., & Oxenham, M. F. (2022). Hydatid disease (*Echinococcosis granulosis*) diagnosis from skeletal osteolytic lesions in an early seventh-millennium BP forager community from preagricultural northern Vietnam. *American Journal of Biological Anthropology*, *177*(1), 100–115.

Weaver, A. A., Beavers, K. M., Hightower, R. C., Lynch, S. K., Miller, A. N., & Stitzel, J. D. (2015). Lumbar bone mineral density phantomless computed tomography measurements and correlation with age and fracture incidence. *Traffic Injury Prevention*, *16*(sup2), S153–S160.

Wu, X., & Schepartz, L. A. (2009). Application of computed tomography in paleoanthropological research. *Progress in Natural Science*, *19*(8), 913–921.

Zhang, L. Z., Du, B. P., Gao, F., & Zhao, L. X. (2021). A micro-CT based study of molar enamel thickness and its distribution pattern in late Miocene *Lufengpithecus lufengensis* from Yunnan in Southwestern China. *Historical Biology*, *33*(10), 2236–2246.

## SUPPORTING INFORMATION

Additional supporting information can be found online in the Supporting Information section at the end of this article.

**How to cite this article:** Towle, I., Loch, C., Oxenham, M., Krueger, K. L., Samir Salem, A., M. M. de Pinillos, Modesto-Mata, M., & Hlusko, L. J. (2024). Technical note: Micro-computed tomography calibration using dental tissue for bone mineral research. *American Journal of Biological Anthropology*, e24952. https://doi.org/10.1002/ajpa.24952

26927691, 0, Downloaded from https://onlinelibrary.wiley.com/doi/10.1002/ajpa.24952 by Universidad De Burgos, Wiley Online Library on [23/05/2024]. See the Terms and Conditions (https://onlinelibrary.wiley.com/terms-and-conditions) on Wiley Online Library for rules of use; OA articles are governed by the applicable Creative Commons License